ELASTODYNAMICS OF A PARALLEL SCHÖNFLIES-MOTION GENERATOR

Zuyu Yin[1], Bruno Belzile[1], Jorge Angeles[1], James Richard Forbes[1]
[1]*Centre for Intelligent Machines and Department of Mechanical Engineering, McGill University, Montréal, Québec, Canada*
Email: zuyuyin@cim.mcgill.ca;bruno@cim.mcgill.ca;angeles@cim.mcgill.ca;james.richard.forbes@mcgill.ca

ABSTRACT

The authors propose a model of the elastodynamics of the *Peppermill Carrier* (PMC), a parallel isostatic Schönflies-motion generator designed for pick-and-place operations. The Cartesian spring and the finite element method are used to build the elastodynamics model of the robot. The stiffness and mass matrices are obtained, as well as the natural frequencies of the robot along a test trajectory—the Adept test cycle—that serves to evaluate the performance of the robot with respect to the operation frequency.

Keywords: Elastostatics; elastodynamics; Schönflies-motion generator.

ÉLASTODYNAMIQUE D'UN GÉNÉRATEUR PARALLÈLE DE MOUVEMENT DE SCHÖNFLIES

RÉSUMÉ

Les auteurs proposent un modèle élastodynamique du *Peppermill Carrier*, un générateur isostatique parallèle de mouvement de Schönflies conçu pour les opérations de transfert. La méthode du ressort cartésien et les éléments finis sont utilisés pour obtenir le modèle élastodynamique du robot. Les matrices de raideur et de masse sont obtenues, ainsi que les fréquences naturelles du robot le long d'une trajectoire test—*Adept test cycle*—ce qui permet d'évaluer la performance du robot en fonction de la fréquence d'opération.

Mots-clés : Élastostatique ; élastodynamique ; générateur de mouvement de Schönflies.

1. INTRODUCTION

Pick-and-place operations (PPOs) encompass many different tasks that involve the moving of an object from one location to another. To produce these operations, serial and parallel robots are commonly used. While the former are known to have large workspaces with respect to their footprint, dexterous capabilities and ease of control, the latter offer many advantages in terms of speed, accuracy, dynamic response, load-carrying capacity, and stiffness. The Selective Compliance Assembly Robot Arm (SCARA) is one of the best-known examples of a serial pick-and-place robot [1]. The set of motions produced by pick-and-place robots is known to form a subgroup, the Schönflies subgroup, of the Lie group of rigid-body motions [2]. These systems are designed with four degrees of freedom (dof), namely three independent translations and one rotation about one axis of fixed orientation.

The H4 robot [3], a parallel Schönflies motion generator (SMG), first proposed by a French-Japanese team, was patented in 2001 [4]. It consists of one moving platform, one base platform and four identical limbs. A detailed review on the structural synthesis of SMG was published by Gogu [5], who claimed that there are totally three kinds of methods used for the structural synthesis of SMG, based on: displacement group theory [6–8]; screw algebra [9–11]; and the theory of linear transformations [12, 13].

Commonly used, four-limb SMG architectures are plagued with limb interference, which results in insufficient rotation ability, limited to an angle smaller than 180° without the use of complex mechanisms inside the moving platform (MP). In the last two decades, many attractive four-limb parallel architectures were proposed, such as H4 [3], I4L [14], I4R [15], Heli4 [16] and PAR4 [17]. An improved version of PAR4 became the Adept Quattro robot [18], which is the fastest parallel robot nowadays.

Compared with four-limb SMGs, two-limb SMGs have smaller footprint and virtually unlimited rotational displacement of the MP, but their stiffness is reduced [19]. Harada and Angeles studied an isoconstrained two-limb SMG, dubbed the Peppermill Carrier (PMC) [20], featuring an architecture proposed by the Lees [21, 22]. The PMC is driven by two identical cylindrical drives (C-drives) [23]. The C-drive design is based on a differential mechanism of the cylindrical subgroup; it produces rotational motion and independent translational motion in the direction of the axis of rotation. A translating Π-joint with a strain-wave-gear (SWG) drive was proposed to enhance the load-carrying capacity of the C-drive [24]. While the objective is to build a manipulator as stiff as possible, deformations are unavoidable due to inertia forces brought about by high-speed/high-acceleration operations. Therefore, manipulators must be considered flexible under these circumstances. However, flexible components of a parallel manipulator will bring about vibration when fast PPOs are conducted. Therefore, the residual vibration after the motion stops will make the settling time longer and positioning accuracy lower. Moreover, vibration will impact on system stability [25].

In this paper, the elastostatics of the PMC is first studied. Then, the trajectory used to obtain numerical data, the *Adept test cycle*, is briefly detailed. Finally, the elastodynamics, including a Fourier analysis, is conducted, the ensuing results then being discussed to assess the stiffness of the PMC.

2. ELASTOSTATICS

2.1. Model

The hypothesis underlying the elastodynamics model of the PMC is summarized as: all links are modelled as rigid bodies, except for the arms and forearms, as illustrated in Fig. 1. The reason for this hypothesis lies in that the latter are significantly more flexible than the other links. Notice that the screws of the C-drives and those of the *Peppermill* cannot be assumed flexible, because a screw joint, just like a prismatic joint, will jam if the joint deforms. Moreover, the flexibility of the strain-wave-gear drive is taken into consideration. While it is not required, the arms and forearms of the PMC have the same lenght. The limbs of the PMC and the SWG-enhanced C-drive are depicted in Fig. 2. The kinematic chain of the PMC is shown in Fig. 1(a). The robot is modelled as an elastostatic system, like the one illustrated in Fig. 1(b). Each of the four springs

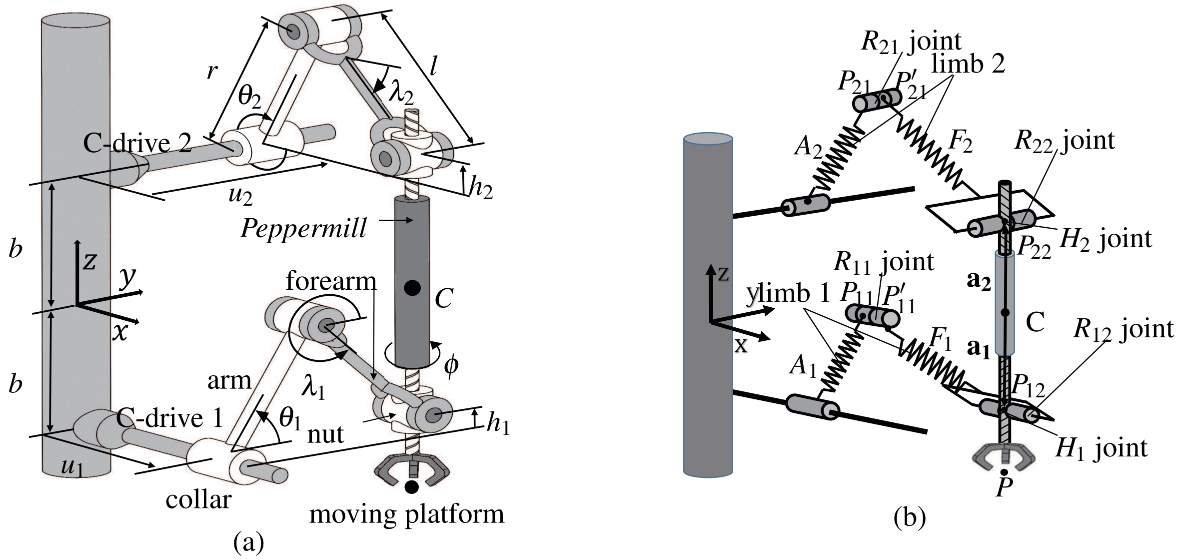

Fig. 1. The models of the PMC: (a) kinematics chain (b) elastostatic model

of the figure is, in fact, a *Cartesian spring*, as defined by Lončarić [26], i.e., a lump of massless, linearly elastic material mounted on a rigid plate and supporting a rigid body on top, illustrated in Fig. 3.

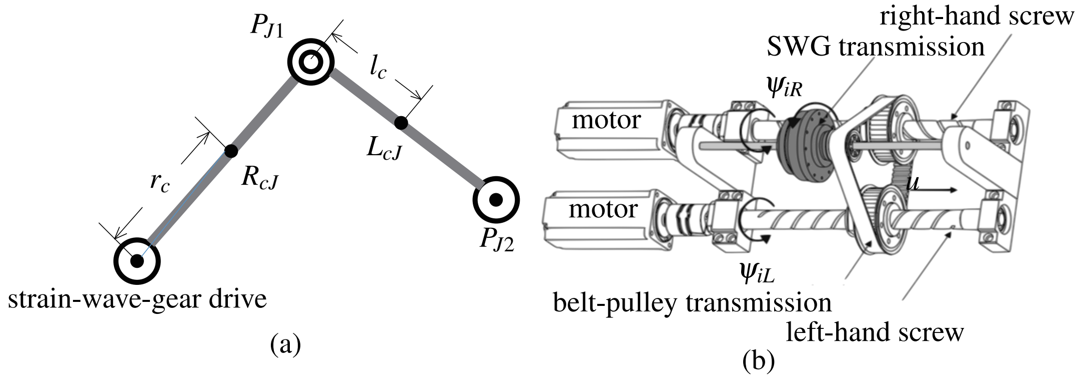

Fig. 2. (a) Side view of limb J, (b) SWG-driven C-drive

The two arms and the two forearms are thus modelled as Cartesian springs. As the rigid body on top of the Cartesian spring is acted upon by an external wrench, the body undergoes a *small-amplitude displacement*, the Cartesian spring then responding with a balancing wrench, identical to the applied wrench, but of opposite sign. Let $\mathbf{q}_{J1}$ be the small-amplitude-displacement (SAD) screw defined at point P_{J1}, where J is the limb label, for $J = 1,2$, as depicted in Fig. 1(b). Furthermore, let $\mathbf{q}_{J2}$ be the SAD screw defined at point P_{J2}. By virtue of the presence of the R_{J1} joint, the SAD screw, defined at point P'_{J1}, becomes

$$\mathbf{q}'_{J1} = \mathbf{q}_{J1} + \delta\beta_J \mathbf{s}_J, \quad \mathbf{s}_J = \begin{bmatrix} \mathbf{e}_J^T & \mathbf{0}^T \end{bmatrix}^T \tag{1}$$

where $\mathbf{e}_J$ is the unit vector parallel to the axis of the R_{J1} joint and $\delta\beta_J$ the small-amplitude relative rotation about the same axis. The forearms are connected to the nuts via R (revolute) joints of horizontal axes. The SAD screws defined at the centre of mass (COM) of the nuts (P_{J2}) and the COM of the *Peppermill* (C) are represented by $\mathbf{q}_{nJ}$ and $\mathbf{q}_m$, respectively. According to the rigidity assumption and the presence of the R

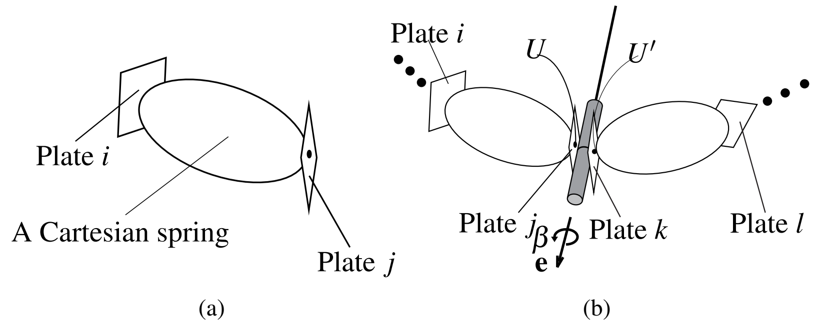

Fig. 3. The concept of Cartesian spring: (a) two rigid plates coupled by a Cartesian spring; (b) the coupling of two Cartesian springs via a R joint

joint, the relationship between $\mathbf{q}_{J2}$ and $\mathbf{q}_{nJ}$ is

$$\mathbf{q}_{J2} = \mathbf{q}_{nJ} + \delta\gamma_J \mathbf{s}_J \tag{2}$$

where $\delta\gamma_J$ is the "small" angle of rotation of the R_{J2} joint, and $\mathbf{s}_J$ is defined in eq. (1). The nuts are connected to the *Peppermill* via H joints of *nominally* vertical axes. The relationship between $\mathbf{q}_{nJ}$ and $\mathbf{q}_m$ is

$$\mathbf{q}_{nJ} = \mathbf{G}_J \mathbf{q}_m + \delta\alpha_J \mathbf{s}_{HJ}, \quad \mathbf{s}_{HJ} = \begin{bmatrix} \mathbf{e}_{HJ}^T & p_J \mathbf{e}_{HJ}^T \end{bmatrix}^T \tag{3}$$

where $\delta\alpha_J$ s the "small" angle of rotation of the H_J joint with respect to the direction of its axis, $\mathbf{e}_{HJ}$ the unit vector of its axis and p_J the pitch of the H_J joint. Moreover, $\mathbf{G}_J$ is the SAD screw *transfer matrix* [27] that takes the SAD screw of one given rigid body from one point to another point of the same body. In the case at hand, from point C to point P_{J2} of the *Peppermill*, $\mathbf{G}_J$ being given by

$$\mathbf{G}_J = \begin{bmatrix} \mathbf{1} & \mathbf{0} \\ -\mathbf{A}_J & \mathbf{1} \end{bmatrix} \tag{4}$$

where $\mathbf{A}_J = \text{CPM}\,(\mathbf{a}_J)$, is the cross-product matrix of vector[2] $\mathbf{a}_J$, stemming from C and ending at P_{J2}.

2.2. The Cartesian Stiffness Matrix

The objective of elastostatic analysis is to obtain the Cartesian stiffness matrix $\mathbf{K}_e$ needed to conduct the modal analysis of the PMC. Matrix $\mathbf{K}_e \in \mathbf{R}^{6\times 6}$ maps the SAD screw of the *Peppermill* into the external wrench applied onto it, which is given by

$$\mathbf{w}_{\text{ext}} = \mathbf{K}_e \mathbf{q} \tag{5}$$

where $\mathbf{w}_{\text{ext}}$ is the external wrench and $\mathbf{q}$ the SAD screw of the *Peppermill*. If we apply a unit external wrench on six different directions separately, the corresponding SAD screws are nothing but the columns of the inverse matrix of the Cartesian stiffness matrix.

Firstly, a unit external force in the x-direction, $\mathbf{w}_{fx}$, is applied at the center of mass C of the *Peppermill*. From the mechanical structure of the PMC, we can find that $\mathbf{w}_{fx}$ will bring about a deformation of the arm and the forearm of limbs 1 and 2. Through the force analysis of the *Peppermill*, balancing forces $\mathbf{f}_{f1p}$ and $\mathbf{f}_{f2p}$ are added on the Peppermill at points P_{12} and P_{22}, respectively. Since the effects of force are mutual, reactive forces $\mathbf{f}_{pf1} = -\mathbf{f}_{f1p}$ and $\mathbf{f}_{pf2} = -\mathbf{f}_{f2p}$ are applied on the forearm of each of limbs 1 and 2, henceforth termed forearm 1 and forearm 2. Therefore, we can obtain the SAD screws of the two forearms in the forms

$$\mathbf{q}_{f1} = \left(\mathbf{K}^{F1}\right)^{-1} \mathbf{w}_{pf1}, \quad \mathbf{q}_{f2} = \left(\mathbf{K}^{F2}\right)^{-1} \mathbf{w}_{pf2} \tag{6}$$

[2]The CPM of $\boldsymbol{A}_J$ is defined as the partial derivative of $\boldsymbol{A}_J \times \mathbf{y}$ with respect to $\mathbf{y}$, $\forall \mathbf{y} \in \mathbf{R}^3$.

where $\mathbf{K}^{F1}$ and $\mathbf{K}^{F2}$ denote the Cartesian stiffness matrices of forearm 1 and forearm 2, respectively, while $\mathbf{w}_{pf1} = \left[\mathbf{m}_{pf1}^T \quad \mathbf{f}_{pf1}^T\right]^T$ and $\mathbf{w}_{pf2} = \left[\mathbf{m}_{pf2}^T \quad \mathbf{f}_{pf2}^T\right]^T$. On the other hand, the forces acting on forearm 1 and forearm 2 will be transferred to arm 1 and arm 2 via corresponding passive revolute joints. The SAD screws of arm 1 and arm 2 are given by

$$\mathbf{q}_{a1} = \left(\mathbf{K}^{A1}\right)^{-1}\mathbf{w}_{f1a1}, \quad \mathbf{q}_{a2} = \left(\mathbf{K}^{A2}\right)^{-1}\mathbf{w}_{f2a2} \tag{7}$$

where $\mathbf{K}^{AJ}$ denotes the Cartesian stiffness matrix of arm J, while $\mathbf{w}_{f1a1} = \mathbf{w}_{pf1}$ and $\mathbf{w}_{f2a2} = \mathbf{w}_{pf2}$. The concept of *SAD-screw transfer matrix* is now recalled. Let $\mathbf{G}_{Jc}$ be given by

$$\mathbf{G}_{Jc} = \begin{bmatrix} \mathbf{1} & \mathbf{0} \\ -\mathbf{A}_{Jc} & \mathbf{1} \end{bmatrix} \tag{8}$$

where $\mathbf{A}_{Jc} = \text{CPM}\ (\mathbf{a}_{Jc})$, vector $\mathbf{a}_{Jc}$ stemming from P_{J2} and ending at C. $\mathbf{G}_{Jc}$ transfers the SAD screw of point P_{J2} to point C, the COM of the *Peppermill*. Therefore, the total deformation caused by the external wrench $\mathbf{w}_{fx}$ is

$$\mathbf{q}_{wfx} = \mathbf{G}_{1c}(\mathbf{q}_{a1} + \mathbf{q}_{f1}) + \mathbf{G}_{2c}(\mathbf{q}_{a2} + \mathbf{q}_{f2}) \tag{9}$$

The SAD screws $\mathbf{q}_{wfy}$, $\mathbf{q}_{wmx}$, $\mathbf{q}_{wmy}$ and $\mathbf{q}_{wmz}$, produced by the unit external wrenches $\mathbf{w}_{fy}$, $\mathbf{w}_{mx}$, $\mathbf{w}_{my}$ and $\mathbf{w}_{mz}$ can be obtained likewise. The deformation $\mathbf{q}_{wfz}$, caused by the unit external force in the z-direction, will be analyzed separately because it is related to the flexibility of the strain-wave-gear drive.

A unit external force $\mathbf{w}_{fz}$ is applied at the center of mass C of the *Peppermill* in the z-direction. Because of the symmetric mechanical structure, each of the wrenches acting on the *Peppermill* by forearm 1, $\mathbf{w}_{f1p}$, and forearm 2, $\mathbf{w}_{f2p}$, equals half of $\mathbf{w}_{fz}$. Therefore, the deformation of forearm J is given by

$$\mathbf{q}_{fJ} = \left(\mathbf{K}^{FJ}\right)^{-1}\mathbf{w}_{pfJ}, \quad J = 1,2 \tag{10}$$

where $\mathbf{w}_{pfJ} = -\mathbf{w}_{fJp}$. On the other hand, the deformation of arm J is given by

$$\mathbf{q}_{aJ} = \left(\mathbf{K}^{AJ}\right)^{-1}\mathbf{w}_{fJaJ}, \quad J = 1,2 \tag{11}$$

where $\mathbf{w}_{fJaJ} = \mathbf{w}_{pfJ}$. As for the angular displacements of the strain-wave-gear drives, which are given by

$$\alpha_J = f_{fJaJ}\cos(\theta_J)r/k_{\text{harm}}, \quad J = 1,2 \tag{12}$$

where f_{f1a1} and f_{f2a2} are the force components of $\mathbf{w}_{f1a1}$ and $\mathbf{w}_{f2a2}$ in the z-direction, θ_1 and θ_2 defined in Fig. 1(a), k_{harm} the torsional stiffness of the strain-wave-gear drive. Therefore, the deformation caused by the strain-wave-gear drives at points P_{11} and P_{21} is

$$\mathbf{q}_{hJ} = \left[\mathbf{0}^T \quad \mathbf{d}_{hJ}^T\right]^T, \quad \mathbf{d}_{hJ} = \left[(J-1)\alpha_2 r\sin(\theta_2) \quad (J-2)\alpha_J r\sin(\theta_J) \quad \alpha_J\cos(\theta_J)\right]^T, \quad J = 1,2 \tag{13}$$

where $\mathbf{0}$ is the three-dimensional zero vector. The deformation caused by the unit external wrench $\mathbf{w}_{fz}$ is

$$\mathbf{q}_{wfz} = \mathbf{G}_{1c}(\mathbf{q}_{a1} + \mathbf{q}_{f1} + \mathbf{q}_{h1}) + \mathbf{G}_{2c}(\mathbf{q}_{a2} + \mathbf{q}_{f2} + \mathbf{q}_{h2}) \tag{14}$$

Since the unit external forces and moments are applied at the COM of the *Peppermill*, the SAD screws are nothing but the columns of the inverse matrix of the Cartesian stiffness matrix of the PMC. Therefore, matrix $\mathbf{K}_e$ is given by

$$\mathbf{K}_e = \left[\mathbf{q}_{wmx} \quad \mathbf{q}_{wmy} \quad \mathbf{q}_{wmz} \quad \mathbf{q}_{wfx} \quad \mathbf{q}_{wfy} \quad \mathbf{q}_{wfz}\right]^{-1} \tag{15}$$

In the above analysis, $\mathbf{K}^{AJ}$ and $\mathbf{K}^{FJ}$ are defined in the base frame and $\bar{\mathbf{K}}^{AJ}$ and $\bar{\mathbf{K}}^{FJ}$ denote the stiffness matrices of arms and forearms defined in the body-fixed frame. $\bar{\mathbf{K}}^{AJ}$ and $\bar{\mathbf{K}}^{FJ}$ are posture-independent, obtained by FEA. $\mathbf{K}^{AJ}$ and $\mathbf{K}^{FJ}$ are posture-dependent, derived from $\bar{\mathbf{K}}^{AJ}$, $\bar{\mathbf{K}}^{FJ}$ by means of similarity transformations in terms of 6×6 rotation matrices, as described below. The coordinate frames of the arms and the forearms are shown in Fig. 4. $\mathscr{F}_0$ represents the fixed frame. $\mathbf{Q}_{J10}$ is the rotation matrix that carries $\mathscr{F}_{J1}$ into $\mathscr{F}_0$. Similarity, $\mathbf{Q}_{J21}$ and $\mathbf{Q}_{J20}$ are the rotation matrices that carry $\mathscr{F}_{J2}$ into $\mathscr{F}_{J1}$ and $\mathscr{F}_{J2}$ into $\mathscr{F}_0$, respectively. A 6×6 rotation matrix $\mathbf{R}_{J10}$ is now introduced to transfer six-dimensional SAD screws from $\mathscr{F}_{J1}$ into $\mathscr{F}_0$:

$$\mathbf{R}_{J10} = \begin{bmatrix} \mathbf{Q}_{J10} & \mathbf{O} \\ \mathbf{O} & \mathbf{Q}_{J10} \end{bmatrix} \tag{16}$$

Similarity, the 6×6 rotation matrices $\mathbf{R}_{J21}$ and $\mathbf{R}_{J20}$ are further introduced:

$$\mathbf{R}_{J21} = \begin{bmatrix} \mathbf{Q}_{J21} & \mathbf{O} \\ \mathbf{O} & \mathbf{Q}_{J21} \end{bmatrix}, \quad \mathbf{R}_{J20} = \begin{bmatrix} \mathbf{Q}_{J20} & \mathbf{O} \\ \mathbf{O} & \mathbf{Q}_{J20} \end{bmatrix} \tag{17}$$

where $\mathbf{R}_{J21}$ and $\mathbf{R}_{J20}$ carry $\mathscr{F}_{J2}$ into $\mathscr{F}_{J1}$ and $\mathscr{F}_{J2}$ into $\mathscr{F}_0$, respectively. Therefore, the relationships between $\mathbf{K}^{AJ}$ ($\mathbf{K}^{FJ}$) and its "overlined" counterpart $\bar{\mathbf{K}}^{AJ}$ ($\bar{\mathbf{K}}^{FJ}$) are readily derived:

$$\mathbf{K}^{AJ} = \mathbf{R}_{J10}^T \bar{\mathbf{K}}^{AJ} \mathbf{R}_{J10}, \quad \mathbf{K}^{FJ} = \mathbf{R}_{J20}^T \bar{\mathbf{K}}^{FJ} \mathbf{R}_{J20} \tag{18}$$

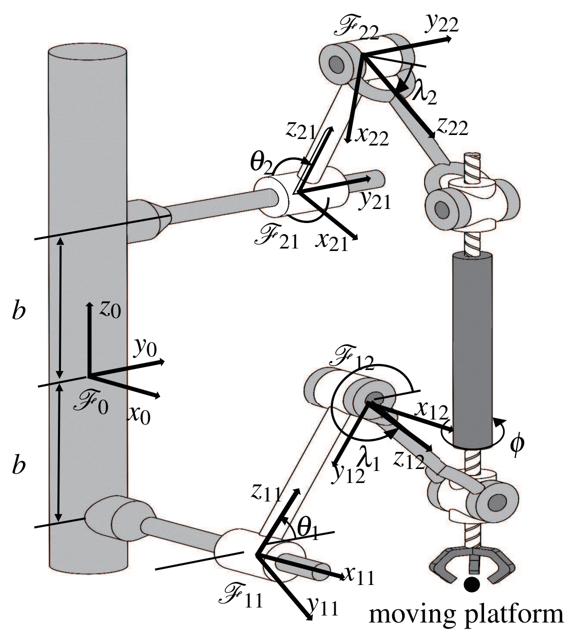

Fig. 4. Cartesian coordinates and body-fixed coordinates

3. ELASTODYNAMICS

To formulate the kinetic energy generated by the flexible-component motion, the generalized coordinates and the generalized velocities are defined below. The independent generalized-coordinate array is defined as

$$\mathbf{q} = \begin{bmatrix} \mathbf{q}_m^T & \mathbf{q}_{11}^T & \mathbf{q}_{21}^T & \delta\gamma_1 & \delta\gamma_2 & \delta\beta_1 & \delta\beta_2 & \delta\alpha_1 & \delta\alpha_2 \end{bmatrix}^T \tag{19}$$

with the corresponding generalized velocity array $\dot{\mathbf{q}}$ following suit:

$$\dot{\mathbf{q}} = \begin{bmatrix} \dot{\mathbf{q}}_m^T & \dot{\mathbf{q}}_{11}^T & \dot{\mathbf{q}}_{21}^T & \delta\dot{\gamma}_1 & \delta\dot{\gamma}_2 & \delta\dot{\beta}_1 & \delta\dot{\beta}_2 & \delta\dot{\alpha}_1 & \delta\dot{\alpha}_2 \end{bmatrix}^T \tag{20}$$

As defined in Subsection 2.1, the components of $\mathbf{q}$ are, respectively, the SAD screws defined at C, P_{11}, P_{21}, and the small-amplitude angle of rotation of the R_{12}, R_{22}, R_{11}, R_{21}, H_1, H_2 joints, Since all the motors are locked at a particular posture, the motion is generated by the deformation of the flexible components. As for the PMC, the kinetic energy is generated by the elastic motion of the arms, the forearms, the nuts and the *Peppermill*, all displayed in Fig. 1(a). Let, for $J = 1,2$, $\dot{\mathbf{q}}_{J1}$, $\dot{\mathbf{q}}'_{J1}$, $\dot{\mathbf{q}}_{J2}$, $\dot{\mathbf{q}}_{nJ}$ and $\dot{\mathbf{q}}_m$ denote the corresponding twists, defined at the points P_{J1}, P'_{J1}, P_{J2}, P'_{J2} and C, respectively, as shown in Fig. 1(b).

As mentioned in Subsection 2.1, a schematic side view of limb J is shown in Fig. 2(a), where the points R_{cJ} and L_{cJ} are the COM of the arm and the forearm, respectively. Let $\dot{\mathbf{q}}_{aJ}$ and $\dot{\mathbf{q}}_{fJ}$ denote the twists defined at the points R_{cJ} and L_{cJ}, respectively. The relationship between $\dot{\mathbf{q}}_{J1}$ and $\dot{\mathbf{q}}_{aJ}$ is

$$\dot{\mathbf{q}}_{aJ} = \mathbf{G}_{J1}\dot{\mathbf{q}}_{J1}, \quad \mathbf{G}_{J1} = \begin{bmatrix} \mathbf{1} & \mathbf{0} \\ -\mathbf{R}_J & \mathbf{1} \end{bmatrix} \tag{21}$$

where $\mathbf{R}_J = \text{CPM}\,(\mathbf{r}_{cJ})$, vector $\mathbf{r}_{cJ}$ stemming from P_{J1} and ending at R_{cJ}. Similarly, the relationships among $\dot{\mathbf{q}}'_{J1}$, $\dot{\mathbf{q}}_{J2}$ and $\dot{\mathbf{q}}'_{fJ}$ are readily derived:

$$\dot{\mathbf{q}}_{fJ} = \mathbf{G}_{J2}\dot{\mathbf{q}}'_{J1} + \mathbf{G}_{J3}\dot{\mathbf{q}}_{J2}, \quad \mathbf{G}_{J2} = \begin{bmatrix} \mathbf{1} & \mathbf{0} \\ -\mathbf{L}_J & \mathbf{1} \end{bmatrix}, \quad \mathbf{G}_{J3} = \begin{bmatrix} \mathbf{1} & \mathbf{0} \\ -\mathbf{L}'_J & \mathbf{1} \end{bmatrix} \tag{22}$$

where $\mathbf{L}_J = \text{CPM}\,(\mathbf{l}_{cJ})$, $\mathbf{L}'_J = \text{CPM}\,(\mathbf{l}'_{cJ})$, vector $\mathbf{l}_{cJ}$ stemming from P'_{J1} and ending at L_{cJ}, its primed counterpart, $\mathbf{l}'_{cJ}$, stemming from P_{J2} and ending at the same point as L_{cJ}. The kinetic energy of arm J is

$$T_J^A = \frac{1}{2}\dot{\mathbf{q}}_{aJ}^T\mathbf{M}^{AJ}\dot{\mathbf{q}}_{aJ}, \quad \mathbf{M}^{AJ} = \begin{bmatrix} \mathbf{I}^{AJ} & \mathbf{O} \\ \mathbf{O} & m^{AJ}\mathbf{1} \end{bmatrix} \tag{23}$$

where $\mathbf{M}^{AJ}$, $\mathbf{I}^{AJ}$ and m^{AJ} are the *von Mises inertia dyad* [28], the inertia tensor and the mass of arm J, respectively. Similarly, the kinetic energy of the forearm, the nut and the *Peppermill* are further introduced:

$$T_J^F = \frac{1}{2}\dot{\mathbf{q}}_{fJ}^T\mathbf{M}^{FJ}\dot{\mathbf{q}}_{fJ}, \quad T_J^N = \frac{1}{2}\dot{\mathbf{q}}_{nJ}^T\mathbf{M}^{NJ}\dot{\mathbf{q}}_{nJ}, \quad T^P = \frac{1}{2}\dot{\mathbf{q}}_m^T\mathbf{M}^P\dot{\mathbf{q}}_m \tag{24}$$

where $\mathbf{M}^{FJ}$, $\mathbf{M}^{NJ}$ and $\mathbf{M}^P$ are the inertia dyads of: forearm and nut of limb J, and of the *Peppermill*, respectively, given by

$$\mathbf{M}^{FJ} = \begin{bmatrix} \mathbf{I}^{FJ} & \mathbf{O} \\ \mathbf{O} & m^{FJ}\mathbf{1} \end{bmatrix}, \quad \mathbf{M}^{NJ} = \begin{bmatrix} \mathbf{I}^{NJ} & \mathbf{O} \\ \mathbf{O} & m^{NJ}\mathbf{1} \end{bmatrix}, \quad \mathbf{M}^P = \begin{bmatrix} \mathbf{I}^P & \mathbf{O} \\ \mathbf{O} & m^P\mathbf{1} \end{bmatrix} \tag{25}$$

The kinetic energy of the PMC is the sum of the kinetic energies of the forearms, the arms, the nuts and the *Peppermill*:

$$T_e = \sum_{J=1}^{2}\left(T_J^A + T_J^F + T_J^N\right) + T^P \tag{26}$$

Substitution of eqs. (21–24) into eq. (26), the expression for the kinetic energy of the PMC becomes,

$$\begin{aligned} T_e = \frac{1}{2}\sum_{J=1}^{2}[&(\mathbf{G}_{J1}\dot{\mathbf{q}}_{J1})^T\mathbf{M}^{AJ}(\mathbf{G}_{J1}\dot{\mathbf{q}}_{J1}) + (\mathbf{G}_{J2}\dot{\mathbf{q}}'_{J1} + \mathbf{G}_{J3}\dot{\mathbf{q}}_{J2})^T\mathbf{M}^{FJ}(\mathbf{G}_{J2}\dot{\mathbf{q}}'_{J1} + \mathbf{G}_{J3}\dot{\mathbf{q}}_{J2}) \\ &+ \dot{\mathbf{q}}_{nJ}^T\mathbf{M}^{NJ}\dot{\mathbf{q}}_{nJ}] + \frac{1}{2}\dot{\mathbf{q}}_m^T\mathbf{M}^P\dot{\mathbf{q}}_m \end{aligned} \tag{27}$$

Moreover, upon differentiation of the two sides of eq. (1), the relationship between $\dot{\mathbf{q}}_{J1}$ and $\dot{\mathbf{q}}'_{J1}$ is obtained:

$$\dot{\mathbf{q}}'_{J1} = \dot{\mathbf{q}}_{J1} + \delta\dot{\beta}_J \mathbf{s}_J \tag{28}$$

By resorting to eqs. (2 & 3), the relationships between $\dot{\mathbf{q}}_{J2}$ ($\dot{\mathbf{q}}_{nJ}$) and its counterpart $\dot{\mathbf{q}}_{nJ}$ ($\dot{\mathbf{q}}_m$) are readily derived:

$$\dot{\mathbf{q}}_{J2} = \dot{\mathbf{q}}_{nJ} + \delta\dot{\gamma}_J \mathbf{s}_J, \quad \dot{\mathbf{q}}_{nJ} = \mathbf{G}_J \dot{\mathbf{q}}_m + \delta\dot{\alpha}_J \mathbf{s}_{HJ} \tag{29}$$

Substitution of eqs. (28 & 29) into eq. (27), leads to

$$\begin{aligned} T_e = \frac{1}{2}\sum_{J=1}^{2} & [(\mathbf{G}_{J1}\dot{\mathbf{q}}_{J1})^T \mathbf{M}^{AJ}(\mathbf{G}_{J1}\dot{\mathbf{q}}_{J1}) + \mathbf{G}_{J2}(\dot{\mathbf{q}}_{J1} + \delta\dot{\beta}_J \mathbf{s}_J) \\ & + \mathbf{G}_{J3}(\dot{\mathbf{q}}_{nJ} + \delta\dot{\gamma}_J \mathbf{s}_J))^T \mathbf{M}^{FJ}(\mathbf{G}_{J2}(\dot{\mathbf{q}}_{J1} + \delta\dot{\beta}_J \mathbf{s}_J) + \mathbf{G}_{J3}(\dot{\mathbf{q}}_{nJ} + \delta\dot{\gamma}_J \mathbf{s}_J) \\ & + (\mathbf{G}_J\dot{\mathbf{q}}_m + \delta\dot{\alpha}_J \mathbf{s}_{HJ})^T \mathbf{M}^{NJ}(\mathbf{G}_J\dot{\mathbf{q}}_m + \delta\dot{\alpha}_J \mathbf{s}_{HJ})] + \frac{1}{2}\dot{\mathbf{q}}_m^T \mathbf{M}^P \dot{\mathbf{q}}_m \end{aligned} \tag{30}$$

The generalized mass matrix of the PMC is the Hessian matrix of T_e with respect to the generalized velocities. This matrix maps the generalized velocity array into the generalized momentum array:

$$\begin{bmatrix} \mathbf{p}_m \\ \mathbf{p}_1 \\ \mathbf{p}_2 \\ p_{12} \\ p_{22} \\ p_{11} \\ p_{21} \\ p_{13} \\ p_{23} \end{bmatrix} = \begin{bmatrix} \mathbf{M}_{11} & \mathbf{M}_{12} & \mathbf{M}_{13} & \mathbf{m}_{14} & \mathbf{m}_{15} & \mathbf{m}_{16} & \mathbf{m}_{17} & \mathbf{m}_{18} & \mathbf{m}_{19} \\ \mathbf{M}_{12}^T & \mathbf{M}_{22} & \mathbf{O} & \mathbf{m}_{24} & \mathbf{0} & \mathbf{m}_{26} & \mathbf{0} & \mathbf{m}_{28} & \mathbf{0} \\ \mathbf{M}_{13}^T & \mathbf{O} & \mathbf{M}_{33} & \mathbf{0} & \mathbf{m}_{35} & \mathbf{0} & \mathbf{m}_{37} & \mathbf{0} & \mathbf{m}_{39} \\ \mathbf{m}_{14}^T & \mathbf{m}_{24}^T & \mathbf{0}^T & m_{44} & 0 & m_{46} & 0 & m_{48} & 0 \\ \mathbf{m}_{15}^T & \mathbf{0}^T & \mathbf{m}_{35}^T & 0 & m_{55} & 0 & m_{57} & 0 & m_{59} \\ \mathbf{m}_{16}^T & \mathbf{m}_{26}^T & \mathbf{0}^T & m_{46} & 0 & m_{66} & 0 & m_{68} & 0 \\ \mathbf{m}_{17}^T & \mathbf{0}^T & \mathbf{m}_{37}^T & 0 & m_{57} & 0 & m_{77} & 0 & m_{79} \\ \mathbf{m}_{18}^T & \mathbf{m}_{28}^T & \mathbf{0}^T & m_{48} & 0 & m_{68} & 0 & m_{88} & 0 \\ \mathbf{m}_{19}^T & \mathbf{0}^T & \mathbf{m}_{39}^T & 0 & m_{59} & 0 & m_{79} & 0 & m_{99} \end{bmatrix} \begin{bmatrix} \dot{\mathbf{q}}_m \\ \dot{\mathbf{q}}_{11} \\ \dot{\mathbf{q}}_{21} \\ \delta\dot{\gamma}_1 \\ \delta\dot{\gamma}_2 \\ \delta\dot{\beta}_1 \\ \delta\dot{\beta}_2 \\ \delta\dot{\alpha}_1 \\ \delta\dot{\alpha}_2 \end{bmatrix} \tag{31}$$

where $\mathbf{p}_m$, $\mathbf{p}_J$, p_{J1}, p_{J2} and p_{J3} are, respectively, the six-dimensional generalized momenta defined at C, P_{J1}, and the generalized angular momenta about the R_{J1}, R_{J2} and H_J joints, $\mathbf{O}$ the 6×6 zero matrix, $\mathbf{0}$ the six-dimensional zero vector, the non-zero blocks of the mass matrix being described below:

$$\begin{aligned} & \mathbf{M}_{11} = \mathbf{G}_1^T\mathbf{G}_{13}^T\mathbf{M}^{F1}\mathbf{G}_{13}\mathbf{G}_1 + \mathbf{G}_1^T\mathbf{M}^{N1}\mathbf{G}_1 + \mathbf{G}_2^T\mathbf{G}_{23}^T\mathbf{M}^{F2}\mathbf{G}_{23}\mathbf{G}_2 + \mathbf{G}_2^T\mathbf{M}^{N2}\mathbf{G}_2 + \mathbf{M}^P \\ & \mathbf{M}_{12} = \mathbf{G}_1^T\mathbf{G}_{13}^T\mathbf{M}^{F1}\mathbf{G}_{12}, \quad \mathbf{M}_{13} = \mathbf{G}_2^T\mathbf{G}_{23}^T\mathbf{M}^{F2}\mathbf{G}_{22}, \quad \mathbf{m}_{14} = \mathbf{G}_1^T\mathbf{G}_{13}^T\mathbf{M}^{F1}\mathbf{G}_{13}\mathbf{s}_1, \\ & \mathbf{m}_{15} = \mathbf{G}_2^T\mathbf{G}_{23}^T\mathbf{M}^{F2}\mathbf{G}_{23}\mathbf{s}_2, \quad \mathbf{m}_{16} = \mathbf{G}_1^T\mathbf{G}_{13}^T\mathbf{M}^{F1}\mathbf{G}_{12}\mathbf{s}_1, \quad \mathbf{m}_{17} = \mathbf{G}_2^T\mathbf{G}_{23}^T\mathbf{M}^{F2}\mathbf{G}_{22}\mathbf{s}_2, \\ & \mathbf{m}_{18} = \mathbf{G}_1^T\mathbf{G}_{13}^T\mathbf{M}^{F1}\mathbf{G}_{13}\mathbf{s}_{H1} + \mathbf{G}_1^T\mathbf{M}^{N1}\mathbf{s}_{H1}, \quad \mathbf{m}_{19} = \mathbf{G}_2^T\mathbf{G}_{23}^T\mathbf{M}^{F2}\mathbf{G}_{23}\mathbf{s}_{H2} + \mathbf{G}_2^T\mathbf{M}^{N2}\mathbf{s}_{H2}, \\ & \mathbf{M}_{22} = \mathbf{G}_{11}^T\mathbf{M}^{A1}\mathbf{G}_{11} + \mathbf{G}_{12}^T\mathbf{M}^{F1}\mathbf{G}_{12}, \quad \mathbf{m}_{24} = \mathbf{G}_{12}^T\mathbf{M}^{F1}\mathbf{G}_{13}\mathbf{s}_1, \\ & \mathbf{m}_{26} = \mathbf{G}_{12}^T\mathbf{M}^{F1}\mathbf{G}_{12}\mathbf{s}_1, \quad \mathbf{m}_{28} = \mathbf{G}_{12}^T\mathbf{M}^{F1}\mathbf{G}_{13}\mathbf{s}_{H1}, \quad \mathbf{M}_{33} = \mathbf{G}_{21}^T\mathbf{M}^{A2}\mathbf{G}_{21} + \mathbf{G}_{22}^T\mathbf{M}^{F2}\mathbf{G}_{22}, \\ & \mathbf{m}_{35} = \mathbf{G}_{22}^T\mathbf{M}^{F2}\mathbf{G}_{23}\mathbf{s}_2, \quad \mathbf{m}_{37} = \mathbf{G}_{22}^T\mathbf{M}^{F2}\mathbf{G}_{22}\mathbf{s}_2, \quad \mathbf{m}_{39} = \mathbf{G}_{22}^T\mathbf{M}^{F2}\mathbf{G}_{23}\mathbf{s}_{H2}, \\ & m_{44} = \mathbf{s}_1^T\mathbf{G}_{13}^T\mathbf{M}^{F1}\mathbf{G}_{13}\mathbf{s}_1, \quad m_{46} = \mathbf{s}_1^T\mathbf{G}_{13}^T\mathbf{M}^{F1}\mathbf{G}_{12}\mathbf{s}_1, \quad m_{48} = \mathbf{s}_{H1}^T\mathbf{G}_{13}^T\mathbf{M}^{F1}\mathbf{G}_{13}\mathbf{s}_1, \\ & m_{55} = \mathbf{s}_2^T\mathbf{G}_{23}^T\mathbf{M}^{F2}\mathbf{G}_{23}\mathbf{s}_2, \quad m_{57} = \mathbf{s}_2^T\mathbf{G}_{23}^T\mathbf{M}^{F2}\mathbf{G}_{22}\mathbf{s}_2, \quad m_{59} = \mathbf{s}_{H2}^T\mathbf{G}_{23}^T\mathbf{M}^{F2}\mathbf{G}_{23}\mathbf{s}_2, \\ & m_{66} = \mathbf{s}_1^T\mathbf{G}_{12}^T\mathbf{M}^{F1}\mathbf{G}_{12}\mathbf{s}_1, \quad m_{68} = \mathbf{s}_{H1}^T\mathbf{G}_{13}^T\mathbf{M}^{F1}\mathbf{G}_{12}\mathbf{s}_1, \quad m_{77} = \mathbf{s}_2^T\mathbf{G}_{22}^T\mathbf{M}^{F2}\mathbf{G}_{22}\mathbf{s}_2, \\ & m_{79} = \mathbf{s}_{H2}^T\mathbf{G}_{23}^T\mathbf{M}^{F2}\mathbf{G}_{22}\mathbf{s}_2, \quad m_{88} = \mathbf{s}_{H1}^T\mathbf{G}_{13}^T\mathbf{M}^{F1}\mathbf{G}_{13}\mathbf{s}_{H1} + \mathbf{s}_{H1}^T\mathbf{M}^{N1}\mathbf{s}_{H1}, \\ & m_{99} = \mathbf{s}_{H2}^T\mathbf{G}_{23}^T\mathbf{M}^{F2}\mathbf{G}_{23}\mathbf{s}_{H2} + \mathbf{s}_{H2}^T\mathbf{M}^{N2}\mathbf{s}_{H2} \end{aligned} \tag{32}$$

R_{J1}, R_{J2} and H_J being passive joints, the angular momentum acting on them vanishes, i.e. $p_{ij} = 0$. The Cartesian mass matrix $\mathbf{M}_e \in \mathbf{R}^{6\times 6}$ maps the small-amplitude twist of the *Peppermill* into the momentum applied onto it, namely $\mathbf{p}_J = \mathbf{0}$. From eq. (31), the Cartesian mass matrix is obtained:

$$\mathbf{M}_e = \mathbf{M}_{11} - \mathbf{M}_{b1}\mathbf{M}_{b2}^{-1}\mathbf{M}_{b1}^T \tag{33}$$

where

$$\mathbf{M}_{b1} = \begin{bmatrix} \mathbf{M}_{12}^T \\ \mathbf{M}_{13}^T \\ \mathbf{m}_{14}^T \\ \mathbf{m}_{15}^T \\ \mathbf{m}_{16}^T \\ \mathbf{m}_{17}^T \\ \mathbf{m}_{18}^T \\ \mathbf{m}_{19}^T \end{bmatrix}^T, \quad \mathbf{M}_{b2} = \begin{bmatrix} \mathbf{M}_{22} & \mathbf{O} & \mathbf{m}_{24} & \mathbf{0} & \mathbf{m}_{26} & \mathbf{0} & \mathbf{m}_{28} & \mathbf{0} \\ \mathbf{O} & \mathbf{M}_{33} & \mathbf{0} & \mathbf{m}_{35} & \mathbf{0} & \mathbf{m}_{37} & \mathbf{0} & \mathbf{m}_{39} \\ \mathbf{m}_{24}^T & \mathbf{0}^T & m_{44} & 0 & m_{46} & 0 & m_{48} & 0 \\ \mathbf{0}^T & \mathbf{m}_{35}^T & 0 & m_{55} & 0 & m_{57} & 0 & m_{59} \\ \mathbf{m}_{26}^T & \mathbf{0}^T & m_{46} & 0 & m_{66} & 0 & m_{68} & 0 \\ \mathbf{0}^T & \mathbf{m}_{37}^T & 0 & m_{57} & 0 & m_{77} & 0 & m_{79} \\ \mathbf{m}_{28}^T & \mathbf{0}^T & m_{48} & 0 & m_{68} & 0 & m_{88} & 0 \\ \mathbf{0}^T & \mathbf{m}_{39}^T & 0 & m_{59} & 0 & m_{79} & 0 & m_{99} \end{bmatrix} \tag{34}$$

4. TRAJECTORY

In order to measure the speed of a pick-and-place robot, a standard industrial task cycle has been defined. The original (non-smooth) cycle is known as the Adept test cycle. This trajectory involves a vertical upward translation of 25 mm, a horizontal translation of 300 mm and a final vertical downward translation of 25 mm. The MP has to move through this trajectory back and forth with a rotation of 180° during the horizontal segment. The MP is at rest at the initial and final locations, the two other locations being intermediate points. The motion between these points takes place along a straight line. Gauthier *et al.* [29] proposed a smooth blending of the non-smooth Adept curve using cubic Lamé curves and an optimum selection of the blending points on the vertical and horizontal segments. This trajectory is the one used in this paper. For the record, the Quattro robot is capable of three cycles per second.

5. FOURIER ANALYSIS

It is essential to obtain the frequency spectrum of a highly repetitive mechanical system because the natural frequencies should be placed outside of it to avoid resonance. The frequency spectrum is obtained by means of Fourier analysis. A periodic function $f(t)$ with a fundamental frequency ω can be represented as:

$$f(t) = \frac{a_0}{2} + \sum_{i=1}^{\infty} a_i \cos(i\omega t) + \sum_{i=1}^{\infty} b_i \sin(i\omega t)$$

where

$$a_0 = \frac{1}{T}\int_{-T/2}^{T/2} f(t)dt,\ a_i = \frac{1}{T}\int_{-T/2}^{T/2} f(t)\cos(i\omega t)dt,\ b_i = \frac{1}{T}\int_{-T/2}^{T/2} f(t)\sin(i\omega t)dt$$

in which i and T are the harmonic index and the period of function $f(t)$, respectively. In this case, the periodic functions are the trajectory functions of the moving platform (MP), namely, the translations along the x-, the y- and the z-axes along with the rotation about the z-axis.

In order to obtain the excitation frequency spectrum and find the highest operation speed whose excitation frequency spectrum is under the first natural frequency of the PMC, the distribution of normalized parameters $|\bar{a}_{xn}|$, $|\bar{a}_{yn}|$, $|\bar{a}_{zn}|$ and $|\bar{a}_{\phi n}|$ with respect to the frequency f when the operation frequency is 1 and 2 cycles/s are plotted in Figs. 5 and 6, respectively.

Modal analysis calls for the stiffness and mass matrices, obtained above. The mathematical model of the robot, at an equilibrium posture, is

$$\mathbf{M}\ddot{\mathbf{x}} + \mathbf{K}\dot{\mathbf{x}} = \mathbf{0} \tag{35}$$

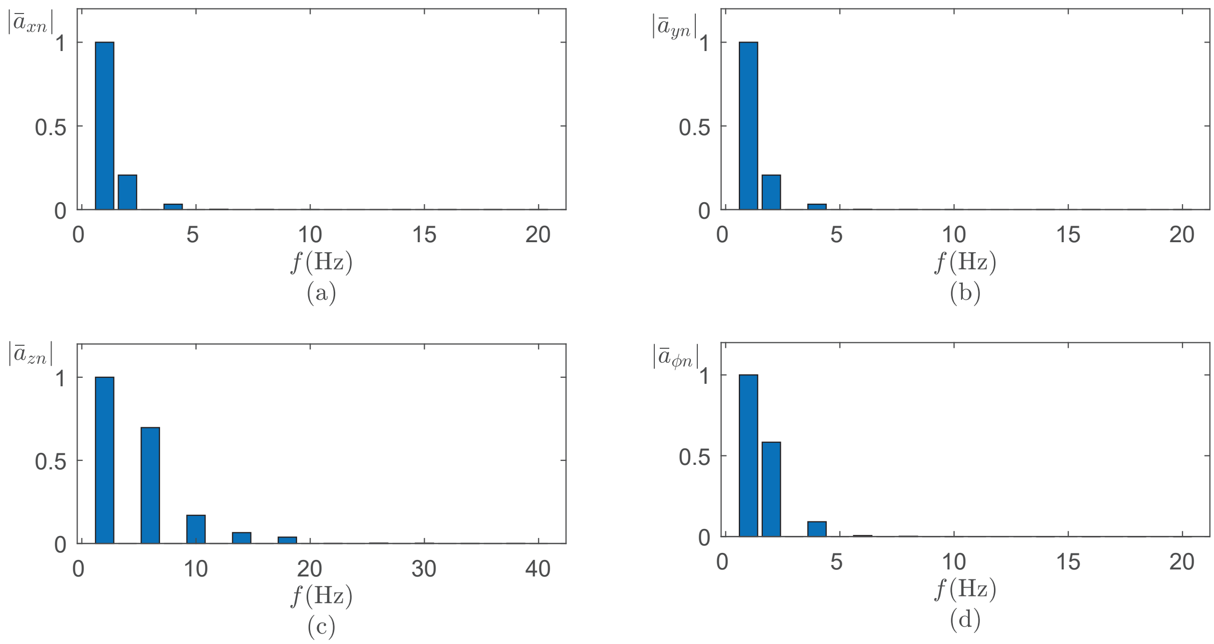

Fig. 5. Amplitudes of the harmonics of the four independent motions vs. natural frequencies (for an operation frequency of 1 cycle/s): (a) translation along the *x*-axis; (b) translation along the *y*-axis; (c) translation along the *z*-axis; (d) rotation about the *z*-axis

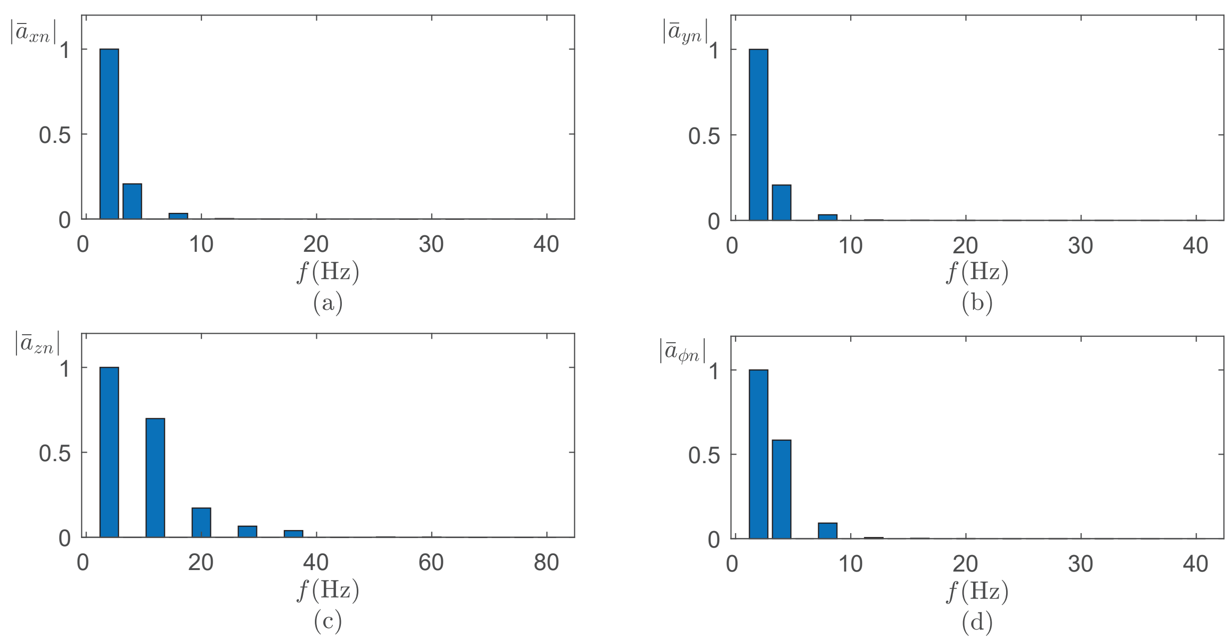

Fig. 6. Amplitudes of the harmonics of the four independent motions vs. natural frequencies (for an operation frequency of 2 cycle/s): (a) translation along the *x*-axis; (b) translation along the *y*-axis; (c) translation along the *z*-axis; (d) rotation about the *z*-axis

where $\mathbf{M}$ and $\mathbf{K}$ are the Cartesian mass and stiffness matrices, $\mathbf{x}$ the SAD screw. To obtain the natural frequencies of the system, the well-known *dynamic-matrix* can be used. One has

$$(\lambda \mathbf{M} + \mathbf{K})\mathbf{u} = \mathbf{0} \tag{36}$$

where λ and $\mathbf{u}$ are, respectively, the eigenvalue and the corresponding eigenvector of the above eigenvalue problem. Therefore, by computing the eigenvalue of $\mathbf{M}^{-1}\mathbf{K}$, the set of values $-\omega^2$ is obtained, with the set ω being that of natural frequencies. It should be noted, however, that the last three components of the six-dimensional eigenvector $\mathbf{u}$ carry units of length, while the first three do not.

With the stiffness ($\mathbf{K}_e$) and mass ($\mathbf{M}_e$) matrices, respectively obtained in Subsection 2.2 and Section 3, the natural frequencies along the Adept test cycle were obtained, as displayed in Fig. 7. Only the first natural frequency is shown, as the subsequent frequencies are well above the first, and thus not significant.

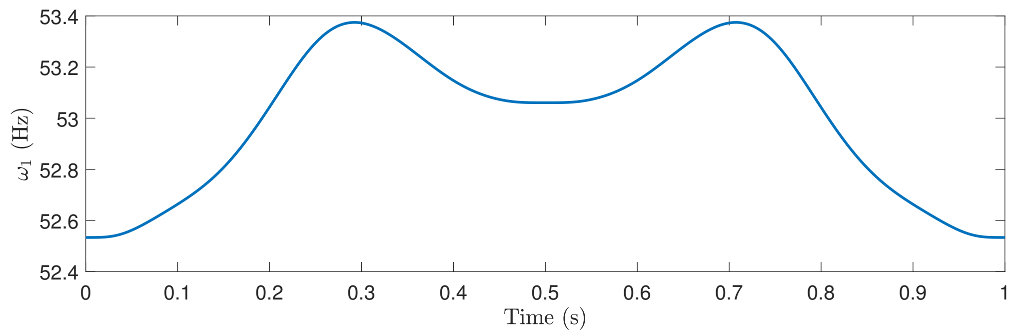

Fig. 7. The evolution of the first natural frequency of the PMC along the test trajectory ω_1 (Hz)

As per Fig. 7, the minimum value of the first natural frequency is 52.5 Hz. According to Fig. 6, the excitation frequency spectrum for an operation frequency of 2 cycles/s, we can see that the translation along the x- and y-axis and rotation about the z-axis are obviously on the safe side. The translation along the z-axis has already reached the limit; hence, resonance will ensue for operation frequencies above this threshold.

6. CONCLUSIONS

The main challenge faced by pick-and-place robots is speed. High-speeds are prone to lead to resonance, which calls for an elastodynamic analysis of the robot to verify that the harmonics of the prescribed trajectory do not lie within the frequency spectrum of the robot structure. The industry standard Adept test cycle was used to obtain numerical data of the frequency content of the cycle at different frequencies. The model and analysis proposed in this paper show that operation frequencies under 3 cycles per second are not problematic. For higher operation frequencies, the current structural design of the robot under development, the PMC, will have to be revised.

REFERENCES

1. H. Makino, A.K. and Yamazaki, Y. "Research and commercialization of scara robot-the case of industry-university joint research and development." *International Journal of Automation Technology*, Vol. 1, pp. 61–67, 2007.
2. Schöenflies, A. *La géométrie du mouvement: exposé synthétique*. Gauthier-Villars et fils, 1893.
3. Pierrot, F. and Company, O. "H4: A new family of 4-DOF parallel robots." In "1999 IEEE/ASME International Conference on Advanced Intelligent Mechatronics, 1999. Proceedings," pp. 508–513. IEEE, 1999.
4. Pierrot, F., Shibukawa, T., Morita, K. et al.. "Four-degree-of-freedom parallel robot." US Patent 6,516,681, February 11 2003.

5. Gogu, G. “Structural synthesis of fully-isotropic parallel robots with Schönflies-motions via theory of linear transformations and evolutionary morphology.” *European Journal of Mechanics-A/Solids*, Vol. 26, No. 2, pp. 242–269, 2007.
6. Hervé, J.M. “New translational parallel manipulators with extensible parallelogram.” In “Proceedings of the 11th world congress in mechanism and machine science,” Vol. 4, pp. 1599–1603, 2004.
7. Angeles, J. “The qualitative synthesis of parallel manipulators.” *ASME Journal of Mechanical Design*, Vol. 126, No. 4, pp. 617–624, 2004.
8. Li, Q., Huang, Z. and Hervé, J.M. “Type synthesis of 3R2T 5-DOF parallel mechanisms using the lie group of displacements.” *IEEE transactions on robotics and automation*, Vol. 20, No. 2, pp. 173–180, 2004.
9. Frisoli, A., Checcacci, D., Salsedo, F. and Bergamasco, M. “Synthesis by screw algebra of translating in-parallel actuated mechanisms.” In “Advances in robot kinematics,” pp. 433–440. Springer, 2000.
10. Gosselin, C.M. “Type synthesis of 3-DOF translational parallel manipulators based on screw theory.”, 2004.
11. Carricato, M. “Fully isotropic four-degrees-of-freedom parallel mechanisms for Schönflies motion.” *The International Journal of Robotics Research*, Vol. 24, No. 5, pp. 397–414, 2005.
12. Gogu, G. “Fully-isotropic T3R1-type parallel manipulators.” In “On Advances in Robot Kinematics,” pp. 265–272. Springer, 2004.
13. Gogu, G. “Singularity-free fully-isotropic parallel manipulators with Schönflies motions.” In “12th International Conference on Advanced Robotics, 2005. ICAR’05. Proceedings.”, pp. 194–201. IEEE, 2005.
14. Krut, O. and Pierrot, S. “Modelling of a 4-axis parallel machine for heavy parts handling.”, 2002.
15. Krut, S., Nabat, V., Company, O. and Pierrot, F. “A high-speed parallel robot for Scara motions.” In “IEEE International Conference on Robotics and Automation,” Vol. 4, pp. 4109–4115. IEEE, 2004.
16. Krut, S., Company, O., Nabat, V. and Pierrot, F. “Heli4: a parallel robot for SCARA motions with a very compact traveling plate and a symmetrical design.” In “IEEE/RSJ International Conference on Intelligent Robots and Systems,” pp. 1656–1661. IEEE, 2006.
17. Nabat, V., Rodriguez, M., Company, O., Krut, S. and Pierrot, F. “Par4: Very high speed parallel robot for pick-and-place.” In “IEEE/RSJ International Conference on Intelligent Robots and Systems,” pp. 553–558, 2005.
18. Pierrot, F., Nabat, V., Company, O., Krut, S. and Poignet, P. “Optimal design of a 4-DOF parallel manipulator: From academia to industry.” *IEEE Transactions on Robotics*, Vol. 25, No. 2, pp. 213–224, 2009.
19. Gauthier, J.F., Angeles, J., Nokleby, S.B. and Morozov, A. “The kinetostatic conditioning of two-limb Schönflies motion generators.” *Journal of Mechanisms and Robotics*, Vol. 1, No. 1, p. 011010, 2009.
20. Harada, T. and Angeles, J. “Kinematics and singularity analysis of a CRRHHRRC parallel Schönflies motion generator.” *CSME Trans*, Vol. 38, No. 2, pp. 173–183, 2014.
21. Lee, P.C. and Lee, J.J. “Singularity and workspace analysis of three isoconstrained parallel manipulators with schoenflies motion.” *Frontiers of Mechanical Engineering*, Vol. 7, No. 2, pp. 163–187, 2012.
22. Lee, P.C., Lee, J.J. and Lee, C.C. “Four novel pick-and-place isoconstrained manipulators and their inverse kinematics.” In “ASME International Design Engineering Technical Conferences and Computers and Information in Engineering Conference,” pp. 1079–1088. American Society of Mechanical Engineers, 2010.
23. Harada, T., Friedlaender, T. and Angeles, J. “The development of an innovative two-DOF cylindrical drive: Design, analysis and preliminary tests.” In “IEEE International Conference on Robotics and Automation (ICRA),” pp. 6338–6344, 2014.
24. Eskandary, P.K. and Angeles, J. “The translating π-joint: design and applications.” *Mechanism and Machine Theory*, Vol. 122, pp. 361–370, 2018.
25. Zhang, Q., Li, C., Zhang, J. and Jin, J. “Active vibration control and coupled vibration analysis of a parallel manipulator with multiple flexible links.” *Shock and Vibration*, Vol. 2016, 2016.
26. Lončarić, J. *Geometrical Analysis of Compliant Mechanisms in Robotics (Euclidean Group, Elastic Systems, Generalized Springs*. Ph.D. thesis, Cambridge, MA, USA. AAI8520241, 1985.
27. Pradeep, A., Yoder, P.J. and Mukundan, R. “On the use of dual- matrix exponentials in robotic kinematics.” *The International Journal of Robotics Research*, Vol. 8, No. 5, pp. 57–66, 1989.
28. Mises, R.V. “Motorrechnung, ein neues Hilfsmittel der Mechanik.” *ZAMM - Journal of Applied Mathematics and Mechanics / Zeitschrift für Angewandte Mathematik und Mechanik*, Vol. 4, No. 2, pp. 155–181, 1924.
29. Gauthier, J.F., Angeles, J. and Nokleby, S. “Optimization of a test trajectory for SCARA systems.” In “Advances in Robot Kinematics: Analysis and Design,” pp. 225–234. Springer, 2008.